

IAC-15.A6.3x28491

PASSIVE OPTICAL SPACE SURVEILLANCE SYSTEM FOR INITIAL LEO OBJECT DETECTION

Paul Wagner
DLR, Germany, paul.wagner@dlr.de

Daniel Hampf
DLR, Germany, daniel.hampf@dlr.de

Wolfgang Riede
DLR, Germany, wolfgang.riede@dlr.de

Institute of Technical Physics, German Aerospace Center (DLR), Pfaffenwaldring 38-40, Stuttgart, Germany

In order to avoid collisions of active satellites with space debris, the low earth orbit (LEO) object population must be continuously scanned and the orbits of all objects must be updated regularly. Passive and active optical observation methods can deliver high accuracy time resolved position measurements of LEO objects allowing accurate orbit determination. Space debris laser ranging stations need accurate a priori orbit information on the position of the object in order to observe it.

The Institute of Technical Physics at the German Aerospace Center in Stuttgart operates an observatory to perform passive as well as active optical measurements to LEO objects. To detect unknown objects a wide-angle imaging system with 15° field of view equipped with an astronomical CCD camera was designed and set up to continuously observe the sky for LEO objects. The system is capable of detecting 25 objects per hour on observation campaigns during twilight at the observatory in city center. The angular coordinates of detected objects are measured roughly without any a priori information.

This paper evaluates the properties of such a "stare" system experimentally. Additionally simulations are performed with ESA PROOF software to validate the measurements and obtain system performance. The simulation show that objects as small as 50 cm can be detected by the system and 60% of all objects larger than 1 m are detected.

I. INTRODUCTION

Background

The Two Line Elements (TLE) database [6] provided by the NASA is currently the largest open source catalogue to access the orbits of objects in earth orbit. This catalog contains about 18000 objects with a size >0.1 m. Thus orbit data of only 65% of all 28000 known objects >0.1 m is available [1]. Because of the large accumulation of active satellites and space debris, the LEO is of special interest. In total 67.5% of all objects in the TLE catalog are LEO objects.

Motivation

To face the increasing risk of collisions of active satellites with space debris, the Institute of Technical Physics at German aerospace center (DLR) in Stuttgart develops a system to measure the position of space debris optically. This is a precise and cost effective alternative to conventional radar facilities used for TLE data generation of LEO objects. The observatory is located at the Uhlandshöhe which is in the city of Stuttgart (altitude: 355m), see Figure 1. Passive optical tracking of LEO objects is possible with an accuracy of 2 arcsec. More information about the receiver telescope and how LEO objects are measured can be found in [2].

Figure 1: DLR observatory can perform passive and active optical measurements using a 17 inch telescope for imaging and single photon counting simultaneously and a 4 inch laser transmitter on an equatorial mount.

Preliminary orbit information of the object under investigation is necessary to perform continuous tracking with the receiver telescope. The accuracy of TLE orbit data is sufficient to detect LEO objects in the field of view (FOV) of the camera connected to the receiver telescope. Then a closed loop keeps the object in the center of the camera.

To perform active optical measurements to unknown space debris objects in LEO their angular coordinates need to be roughly measured and predicted by a separate system. Therefore a "stare and chase" system is under development. In this paper the stare system is described and its performance is compared with simulations.

II. STARING SYSTEM DESIGN

To perform the initial object detection a passive optical system is used. The disadvantages are the dependency on good weather conditions and that objects need to be illuminated by the sun. The advantages of a passive optical system are the low system cost and easy operability. One man is able to perform observations. This allows the operation of several systems across the globe to overcome local weather dependency and all day observation. By increasing the FOV of the passive optical system, the detection probability of a LEO object is increased. Furthermore the resolution (or pixel scale) of the system needs to be high enough to allow a precise preliminary prediction. The following parameters affect the overall system performance;

- Large FOV – higher detection rate
- Large pixel scale (focal length / pixel size) – higher accuracy of angular measurement
- Large aperture – smaller (faint) objects detectable and higher detection efficiency
- Faster frame rate and image processing – shorter prediction overhead time and higher prediction accuracy

The expected minimum angular resolution to capture the object in the FOV of our receiver telescope (16 arcmin by 19 arcmin) is few dozen arcsec per pixel. Additionally the prediction has to be fast enough that the receiver telescope can "catch" the object in its FOV and perform measurements before the objects is below the horizon.

An overview of the proposed system can be found in Figure 2. The staring camera detects LEO objects, measure the angular coordinates and perform a rough prediction. Using this information shall allow precise position measurement using passive and active optical methods with a larger telescope. Figure 3 shows the region covered by our staring system. At a height of 800 km an area of 200 km² is observed. Figure 4 shows the staring camera mounted at the observatory. The astronomic CCD camera ProLine16803 from Finger Lake Instruments is used as staring camera. It shows low system noise (of $14e^-$ per pixel) has a large sensor array of 36.8^2 mm² but a slow shutter including long read out time results in a slow frame rate of 0.2 Hz (full resolution). Using a binning of 2 increases the shutter frequency up to 0.8 Hz. Therefore the camera will be used with binning 2 (2048 px by 2048 px effective resolution) only. The system properties of the staring system and the receiver telescope can be found in Table 1. Further information about the design of the receiver telescope can be found in [2].

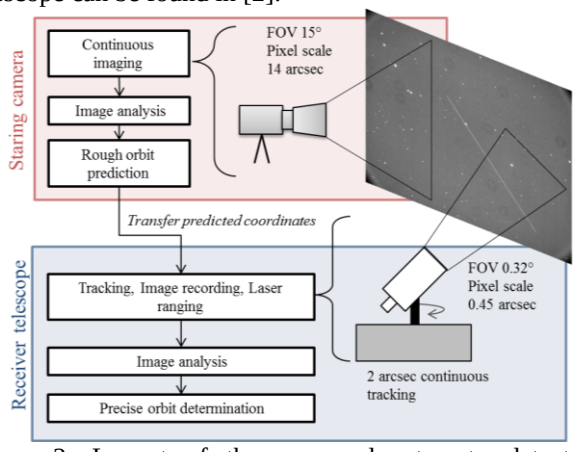

Figure 2: Layout of the proposed setup to detect unknown objects with a staring camera and send predicted coordinates to a separated system to detect the object with the receiver telescope.

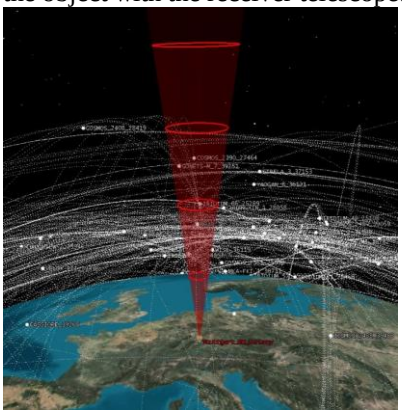

Figure 3: An illustration of satellite orbits (white lines) and the region in LEO covered by the staring cam (red cone) as it is used during observation campaigns. Red circle illustrates the area observed at 500, 1000, 1500 and 2000km height. Copyright: AGI [12]

Figure 4: The staring camera system is mounted on a manual equatorial mount and records images continuously. Angular coordinates of LEO objects passing the FOV are measured which will allow rough orbit predictions.

Properties	Staring system	Receiver telescope
Sensor size [mm²]	36.8 x 36.8	16.6 x 14.0
Pixels	4096 x 4096	2560 x 2160
Pixel size [µm]	9	6.5
Focal length [mm]	135	2939
Aperture diameter [mm]	67.5	432
Field of view (FOV)	15° x 15°	0.32° x 0.27°
Pixel scale (binning 2) [arcsec/px]	13.75 (27.5)	0.46 (0.92)

Table 1: Properties comparison of the two systems used at the DLR observatory in Stuttgart. The staring camera is the wide angle system which should allow the main telescope to "catch" or "chase" detected LEO objects.

The staring camera observes a fixed section of the night sky (fixed Alt-Az) and records images continuously. Due to high angular velocities of LEO objects up to 0.45 °/s the objects are recorded as tracks whereas stars are imaged as a point using 1s shutter speed. A composition of 20 recorded images showing three different objects is given in Figure 5. The objects positions are measured by determine the track start and end point and converting those camera coordinates to Ra-Dec coordinates using the star positions as reference. Using the exposure time and track length allows to determine the angular velocity. Recording an object several times allow determining the direction of flight. Thus using two images containing the same object allows a rough prediction of objects orbit for the next seconds.

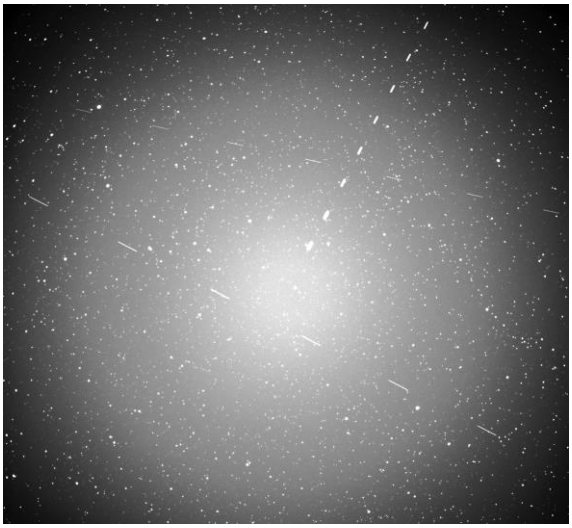

Figure 5: A composite image of 20 single frames recorded by the staring camera during a 60s observation time. Each frame has an exposure time of 1s using FLI CCD camera with Canon 135 mm f/2 lens headed to zenith. It was recorded on 17.04.2014 20:46 (UTC) and three different LEO objects passing the field of view.

The camera is mounted on a manual equatorial mount. Precise Altitude-Azimuth line of sight direction is determined via Pin Point Astronomical position software.

A optic with a focal length of 135mm and a F-number of 2 is used which results in a FOV of 15° by 15° with a scale of 13.75 arcsec/px, respectively 27.5 arcsec/px using binning 2.

The camera trigger is connected to a self-developed GPS timer which allows precise time stamp recording. This is necessary for a rough orbit prediction to chase the object with the receiver telescope.. The following describes how images are processed to measure the object position.

III. IMAGE PROCESSING

Severall steps need to be done to detect the recorded track. Image recording as well as subsequent image processing and further analysis are performed within the Python programming environment.

All the detected images show strong vignetting, which is corrected first. Then a binarisation is performed and a subsequent blob (Binary Large OBject) detection (also called labelling) allows to separate the stars from the tracks in the image. Afterwards all found tracks during an observation night and their properties (e.g. start/end position, corresponding start/stop time, shape, …) are recorded. Each orbital object can be recorded in on many images while it passes the field of view and sometimes more then one orbital object is in the FOV of the camera, see Figure 5. Therefore all tracks need to be correlated to actuall orbital objects. A TLE catalog comparison is performed to check if an object in the TLE database is expected in the FOV of the camera once a track was deteckted. An overview can be found Figure 6.

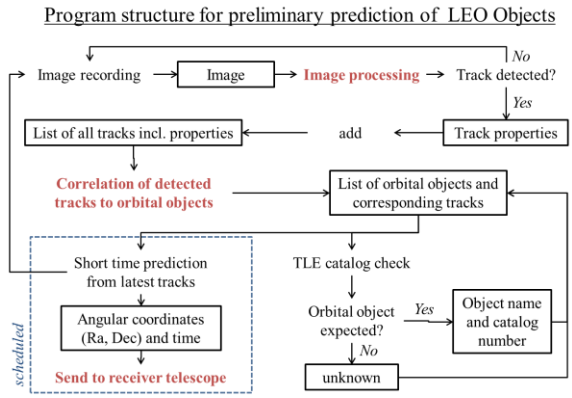

Figure 6: Overview of the program structure to detect orbital objects from continuous image recording. First tracks are extracted from image, then detected tracks are correlated to orbital object which are compared with the TLE catalogue. In future stage the system shall perform reliable predictions.

Vignetting correction

The first step is to correct the image vignetting or shading. Figure 7 (left) shows a typical image as recorded by the camera. Due to operation at dusk and light pollution (high clouds) from the city the vignetting characteristic changes by time. That is why a dynamic vignetting correction is implemented. First all bright details like stars and the track are erased using a minimum filter, see Figure 7 (center). The result is subtracted from the original image, see Figure 7 (right).

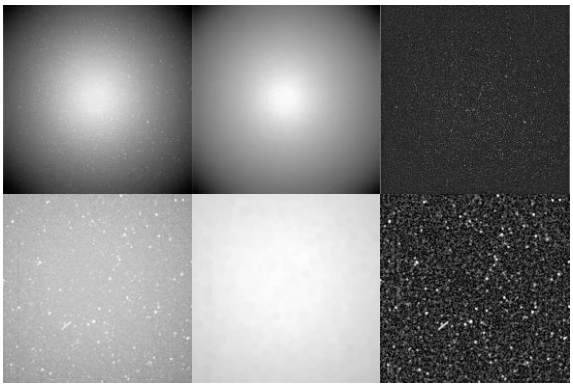

Figure 7: The original (left) image shows a high amount of vignetting. Using a minimum filter erases all details (centre) which allows subtracting the background illumination from the original image to obtain a corrected image (right). While the upper row shows the complete image, the second row shows only the central part.

Track detection

Once background illumination is earased from the image the track analysis can be perfomed using blob analysis (or labeling). Therefore the corrected grayscale image, Figure 7 (right), is converted to a binary image using a global threshold of 2 sigma above the average background noise, see figure Figure 8 left. To identify tracks in the binary image all small binary objects in the image (which result from faint stars and noise) are removed first by deleting all biniary objects with an area smaller then 80px, see figure Figure 8 center. To extract the track from remaining binary objects, the properties (or features) of each binary object are evaluated [13]. Subsequently all binary objects with an eccentricity smaller than 0.92 are deleted.

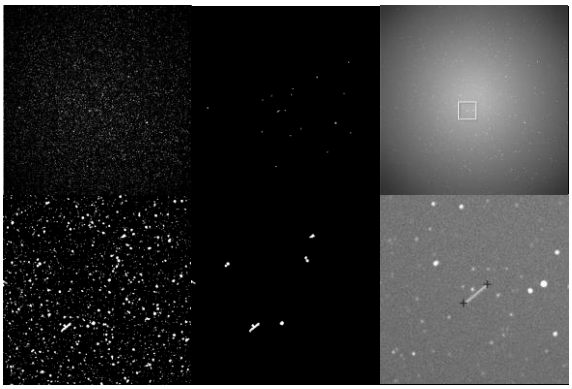

Figure 8: The binary image (left) shows many objects resulting from noise, stars and tracks. After deleting small binary objects (centre) only a few binary objects are left. After measuring the properties of each object the tracks can be identified and their position measured (right).

To identify the flight direction of each orbital object, at least two images containing the same object have to be recorded.

To check if detected tracks of subsequent images belong to one and the same orbital object, the properties of the tracks have to be compared. The following properties are compared:

- Track length
- Start/end position
- Start/end time
- Orientation

Tracks in subsequent images with coinciding properties are correlated to one orbital object. Using this correlation a false detected track (track with properties not found in subsequent images) will not be counted as an orbital object. Only high clouds or high flying aircrafts can disturb the program. An aircraft checker is planned to be implemented at the observatory to overcome this problem.

Finally it is checked if the detected object can be found in the TLE catalog. Therefore the positions and flight directions of all objects in the TLE catalog are calculated at the time at which an object was detected by the staring camera. If there is no TLE object with corresponding properties to the detected object, the detected object is not catalogued in the TLE database. All data is then written into a file which allows checking false detections and further analysis.

IV. SIMULATION

For system setup evaluation it is useful to simulate observation campaigns which allows to determine necessary system specifications.

As simulation software ESA's PROOF [4] was used. This software simulates an observation sensor (radar or optical) and determine how many orbital objects it detects during an observation campaign. Table 2 shows the system parameters used for the simulation. The software simulates passes of orbital objects randomly based on the well-known population model MASTER-2009 [5]. An optical model is included which takes the quantum efficiency of the camera, atmospheric absorption and the point spread function (PSF, of the whole system including turbulence) into account. The measurements presented in the next paragraph are compared with corresponding simulations.

Parameter	Value
FOV [°]	15.27
Diameter of aperture [m]	0.0675
Number of pixels per row	2048
Pixel size [µm]	18
Pixel scale [arcsec/px]	27.5
FWHM (PSF) [px]	2
Exposure time [s]	1
Signal to Noise Ratio (SNR)	3
Read out noise [e^-]	9
Dark noise [e^-/s]	0.07
Monte Carlo runs	100
Number of simulation steps per object	300
smallest Object diameter [m]	0.01
largest Object diameter [m]	100
Geodetic latitude [°]	48.78253
Geodetic longitude [°]	9.19641
Geodetic altitude [m]	355
Azimuth / Right Ascension	230°
Elevation / Declination	88°
Range of objects [km]	200 – 4000

Table 2: Summary of settings used for simulation. The settings are either taken from data sheets or are measured.

V. MEASUREMENTS

The camera is pointed to zenith and 1 s exposure time is used for all measurements. The binning is set to 2 to reduce the datarate, image processing time and to increase shutter frequency. As longer data transfer and image processing takes as lower is the probarbility to catch the detected object with the reciver telescope. A higher frame rate and shorter image processing time increases the porbarbility of a succsessfull chasing.

All measurements were started at astronomical twilight conditions between February and August 2015. Duration varied from 20min up to 2.5h each night. The total observation time was 23.5h which result in 13500 images. All images were analyzed and detected orbital objects were compared with the TLE catalog. The TLE catalog checker was available for the later measurements. 330 of 427 detected objects could be found in the TLE catalog. This means that 23% are non-cataloged objects. The detection rate was 24 objects per hour and varied by 4.7 objects per hour (standard deviation). All measurements of each night were simulated with exactly the same simulation parameter. The detection rate fluctuates much higher than in the measurements with 7.9 objects per hour. But in total the simulation differs only 2% from the measurements. This shows that the simulation is a good tool to compare general system properties. Table 3 shows a summary of the results. All measurements are listed in IX Appendix (1).

Measurements	Objects detected	568
	Detection rate [obj/h]	24.2 ±4.7
	Detected TLE Obj.	330 (of 427)
	Not cataloged obj. percentage	23 % ± 13 %
Simulation	Objects detected	580
	Detection rate [obj/h]	24.7 ±7.9
	Simulation/ Measurement	1.02 ±0.44
	smallest Object [m]	0.55 ±0.15

Table 3: Summary of performed measurements between February and August 2015 in comparison with simulations. Total observation time was 23.471 h with 13500 recorded images. Line of sight was altitude=88°, azimuth=230°.

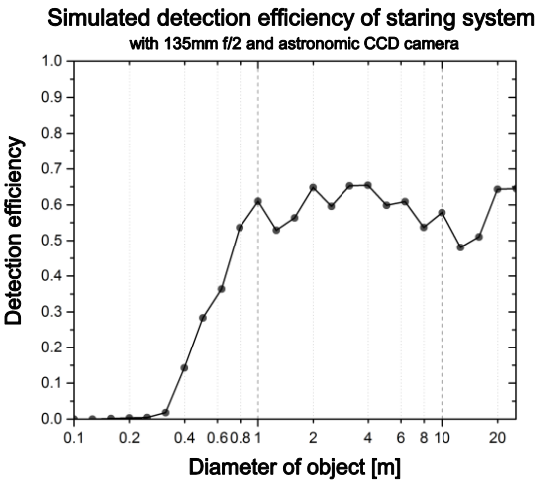

Figure 9: Simulated detection efficiency of LEO objects of the staring system as function of the object diameter.

The simulation allows analyzing the results depending on the object size. According to the

simulation the smallest detected object at each night has a diameter ranging from 0.4m to 0.7m.

Furthermore the simulation gives the number of objects which passed the FOV and the number of detected objects. This allows calculating the detection efficiency depending on the object size. Figure 9 shows the detection efficiency of the system used for the measurements. The maximum efficiency is 65% and drops to 30% at an object size of 0.5m.

VI. CONCLUSION

In this paper the setup and properties of our staring system dedicated to monitor LEO objects is presented. It was demonstrated a simple setup of a large area CCD camera in combination with a 135mm lens is already able to detect 24 LEO objects per hour with an object size down to 0.4m. Comparison with ESA's PROOF simulation software has shown that the simulation is a great tool to compare overall system properties like detection rate. Additionally the software can provide more information like detection efficiency depending on object size.

The simple setup of a camera with an array detector and an optical lens allows a variety of different optical system combinations like high detection rates (but low accuracy) combined with a high accuracy measurement. Compared to overall system cost the staring system is an affordable addition to a laser ranging system.

Future potential

Future development on the system contains integration of the staring cam with the receiver telescope to perform precise passive and active optical measurements. First tests indicate that it is possible to "catch" the detected objects in the receiver telescope FOV. For reliable catching further improvement of the image processing speed is necessary.

The system is just the first step and the image analysis can be speed up by using multi-core and GPU processing. In Reference [8] is shown that a fast faith track analysis is generally possible. Further improvement is possible by increasing the frame rate using high resolution CMOS detectors allowing a faster and better prediction of the objects position.

Due to low cost and easy operability a multiple aperture system and systems with complementary properties can be set up easily.

VII. ACKNOWLEDGEMENTS

This work has been supported by the BAAINBw.

VIII. REFERENCES

[1] H. Klinkrad, „Space Object Catalogs", SSA Conference 2006, Colorado Springs (15 Sep 2006)

[2] Daniel Hampf, Paul Wagner, Wolfgang Riede, "Optical technologies for the observation of low Earth orbit objects", *Proc. of IAC 2014 (Toronto),* 2014

[3] A. Milani, A. Villani, M. Stiavelli, "Discovery of very small asteroids by automated trail detection", *Earth, Moon and Planets 72: 257-262, Kluwer Academic Publishers*, (1996)

[4] Johannes Gelhaus and Sven Flegel and Carsten Wiedemann, „Program for Radar and Optical Observation Forecasting", *Institute of Aerospace Systems, TU Braunschweig, Final Report, M09/GEN-WP3200*, 2011

[5] Svel Flegel, "Maintenance of the ESA MASTER Model", *Institute of Aerospace Systems, TU Braunschweig, Final Report, 21705/08/D/HK*, 2011

[6] www.space-track.org/

[7] James R. Shell, „Optimizing orbital debris monitoring with optical telescopes",*Proceedings of the 2009 AMOS Technical Conference*, 2009

[8] Zimmer, Peter C., Ackermann, Mark R., McGraw, John T. "GPU Accelerated Faint Streak Detection for Uncued Surveillance of LEO*"*, *Proceedings of the 2013 AMOS Technical Conference*, 2013

[9] Zimmer, Peter C., Ackermann, Mark R., McGraw, John T., "Demonstration of Uncued Surveillance of LEO", *Proceedings of the 2014 AMOS Technical Conference*, 2014

[10] Sun-youp Park, et. al., "Data Reduction Algorithm for Optical Wide Field Patrol(OWL)", *Proceedings of the 2014 AMOS Technical Conference*, 2014

[11] T. Yanagisawa, H. Kurosaki, H. Oda, M. Tagawa, "Ground-based optical observation system for LEO objects", *Advances in Space Research 56 (2015) 414–420*, 2015

[12] Satellite Tool Kit by Analytical Graphics Inc. (www.agi.com)

[13] Wilhelm Burger, Mark James Burge, „Digitale Bildverarbeitung", *ISBN-13 978-3-540-21465-6 Springer Berlin Heidelberg New York*, 2005

[14] Guillaume Blanchet, Hervé Haag, Laurent Hennegrave, François Assémat, Sophie Vial, Etienne Samain, "Laser ranging for effective and accurate tracking of space debris in low earth orbits", *Proc. '6th European Conference on Space Debris' Darmstadt, Germany,* 22–25 April 2013

[15] I. Prochazka, K. Hamal, M. Nemec, G. Kirchner, F. Koidl, W. Voller, "Space objects optical tracking 3D solution", *Proceedings of the Fourth European Conference on Space Debris, Darmstadt, Germany*, 18-20 April 2005

IX. APPENDIX

(1) List of all Measurements with corresponding simulation

Measurement										Simulation			
Observation start date [YYYY-MM-DD hh:mm:ss]	Duration [h]	Alt-Az	Gap time [s]	Objects detected	Detected TLE Obj.	Detection rate [obj/h]	Unknown percentage	Number of Images	Detected	Detection Rate	Simulation/ Measurements	smallest Object [m] (according simulation)
11.02.2015 18:08	0.8	88-228	3	20		25.0		718	20	25.0	1.00	0.38
07.04.2015 21:18	0.75	88-228	5	22		29.3		462	15	20.0	0.68	0.41
08.04.2015 21:30	0.517	88-228	5	13		25.1		323	11	21.3	0.85	0.64
08.04.2015 21:37	0.1	88-228	8	3		30.0		40	0	0.0	0.00	
09.04.2015 21:07	1.18	88-228	5	31		26.3		706	31	26.3	1.00	0.43
12.04.2015 20:53	1.25	88-228	7	37		29.6		536	39	31.2	1.05	0.45
20.04.2015 22:01	0.217	88-228	6	6		27.6		107	8	36.9	1.33	0.54
20.04.2015 22:14	0.267	88-228	4	9		33.7		190	10	37.5	1.11	0.54
07.05.2015 22:33	0.3	88-228	5	6	6	20.0	0.00	187	8	26.7	1.33	0.80
30.06.2015 22:49	2.36	88-228	5	45	37	19.1	0.18	1299	39	16.5	0.87	0.68
01.07.2015 22:40	1.95	88-228	7	47	42	24.1	0.11	817	43	22.1	0.91	0.41
10.07.2015 20:54	2.28	88-228	4	74	63	32.5	0.15	1636	56	24.6	0.76	0.38
20.08.2015 21:48	0.25	88-230	9	6	4	24.0	0.33	86	7	28.0	1.17	0.83
21.08.2015 21:22	2.1	74-266	9	25	19	11.9	0.24	745	64	30.5	2.56	0.40
22.08.2015 21:27	0.75	75-265	9	17	16	22.7	0.06	278	19	25.3	1.12	0.58
22.08.2015 22:13	0.9	75-265	3	23	11	25.6	0.52	773	32	35.6	1.39	0.36
25.08.2015 21:21	1.1	75-265	4	27	21	24.5	0.22	794	32	29.1	1.19	0.67
25.08.2015 00:00	0.25	75-265	6	6	5	24.0	0.17	132	9	36.0	1.50	0.62
25.08.2015 00:00	0.25	75-265	7.5	7	5	28.0	0.29	106	5	20.0	0.71	0.80
26.08.2015 21:30	2.3	75-265	5	60	46	26.1	0.23	1395	51	22.2	0.85	0.29
29.08.2015 21:20	2.1	75-265	5	54	36	25.7	0.33	1282	43	20.5	0.80	0.70
30.08.2015 21:13	1.5	75-265	4	30	19	20.0	0.37	888	38	25.3	1.27	0.63
Sum	23.471			568	330			13500	580			
Mean						24.2	0.23			24.7	1.02	0.55
Deviation						4.7	0.13			7.9	0.45	0.15